PAPER

Check for updates

The role of high-energy phonons in electron–phonon interaction at conducting surfaces with helium-atom scattering

G. Benedek, [ID] [ab] J. R. Manson [ID] [ac] and Salvador Miret-Artés [ID] *[ad]

In previous works it has been shown that the Debye–Waller (DW) exponent for Helium atom specular reflection from a conducting surface, when measured as a function of temperature in the linear high-temperature regime, allows for the determination of the surface electron–phonon coupling. However, there exist a number of experimental measurements that exhibit non-linearities in the DW exponent as a function of the surface temperature. Such non-linearities have been suggested as due to vibrational anharmonicity or a temperature dependence of the surface carrier concentration. In this work, it is suggested, on the basis of a few recent experimental data, that the deviations from linearity of the DW exponent temperature-dependence, as observed for conducting surfaces or supported metal overlayers with the present high-resolution He-atom scattering, permit to single out the specific role of high-energy phonons in the surface electron–phonon mass-enhancement factor.

1 Introduction

In 1929 Otto Stern with his helium-atom scattering (HAS) experiments from a crystal surface filled two needs with one deed: proving the quantum particle-wave duality for atoms and the ordered structure of crystal surfaces. The development of supersonic monochromatic ($\Delta E < 0.5$ meV) He-beam spectrometers paved the way to high-resolution momentum-resolved spectroscopy of surface dynamics on the atomic scale. More needs fulfilled and envisaged by Stern! Unlike thermal neutrons and X-rays, thermal neutral He atoms probe the surface ~ 0.3 nm away from the first atomic plane, and exchange energy and momentum with the solid atoms only *via* the interposed electrons. Thus, phonons are detected *via* the electron–phonon (e–ph) interaction, and not just at the surface, but possibly as deep below the surface as the range of that interaction. This sort of quantum sonar allows for the direct measurement of the e–ph coupling strength for each individual phonon (mode-λ spectroscopy),[1] and for ultimately answering the question about phonon-mediated pairing in (2D-) superconductors: whos doing the job? The venerable concept of

Debye–Waller (DW) factor, by which Piet Debye (1913) and Ivar Waller (in his 1923 thesis) correctly attributed to thermal vibrations the attenuation of Roentgen rays, in the case of HAS from conducting surfaces presently allows for a direct measurement of the e–ph mass-enhancement factor λ – a basic parameter for conducting materials.[2] This is made possible by the theoretical demonstration that the linear decay of the DW exponent $2W(T)$ with the surface temperature T is approximately proportional to λ, with the proportionality constant estimated from known parameters of the surface.

In the last decade, measurements of the HAS-DW factor $2W(T) = \ln[I_{00}(T)/I_{00}(0)]$ associated with the specular scattering intensity $I_{00}(T)$ have provided, through the temperature dependence, reliable values of λ for a variety of surfaces, ranging from those of ordinary metals[3] and metal overlayers[4] to the surface of topological[5–7] and multidimensional[8] materials, 2D superconductors[9,10] and graphene.[11] The new potentialities of HAS spectroscopy have been reviewed in a recent Perspective.[12] There is, however, a substantial difference between the temperature dependence of the DW exponent for the direct collision of the probe particles with the atomic nuclei or cores, as for thermal neutron or X-ray scattering (and also for atom scattering from an insulating surface), and that of the DW exponent for atom scattering from a conducting surface. While in the former cases the scattering particles directly probe the thermal vibrations of the atoms, where the low-energy phonons play a major role, in the latter the scattering atoms probe the charge density oscillations induced by the atomic vibrations, and therefore weighted by the electron–phonon coupling,

[a] *Donostia International Physics Center (DIPC), Paseo Manuel de Lardizabal, 4, 20018 Donostia-San Sebastian, Spain*

[b] *Dipartimento di Scienza dei Materiali, Università di Milano-Bicocca, Via Cozzi 55, 20125 Milano, Italy*

[c] *Department of Physics and Astronomy, Clemson University, Clemson, South Carolina 29634, USA*

[d] *Instituto de Física Fundamental, Consejo Superior de Investigaciones Científicas, Serrano 123, 28006 Madrid, Spain. E-mail: s.miret@iff.csic.es*

This journal is © the Owner Societies 2022

Phys. Chem. Chem. Phys., 2022, **24**, 23135–23141 | 23135

which is generally stronger for the high-energy phonons. In the former cases, the temperature dependence of the DW exponent is generally well accounted for by a Debye model for lattice dynamics, due to the prominence of low-energy acoustic modes, while for HAS from a conducting surface the high-energy phonons, *e.g.*, the optical phonon branches occurring for polyatomic surface unit cells, are expected to play a detectable effect in the measured $2W(T)$. If only acoustic modes were important, the DW exponent would be perfectly linear in T for T well above the Debye temperature. A deviation from linearity, *e.g.*, an increase in the slope of $2W(T)$ *versus* T above a certain temperature T_h is a signature that high-energy phonons of energy about $k_B T_h$ are being involved, and the size of such deviation depends on their electron–phonon coupling.

High-resolution HAS (or even better ³He spin-echo) measurements of $2W(T)$ can therefore allow to weight the electron–phonon coupling of high-energy phonons as compared to low-energy phonons, where by high- *versus* low-energy we may intend optical *vs.* acoustic phonons, or substrate *vs.* overlayer phonons (or *vice versa*), in case a soft (hard) overlayer on a hard (soft) substrate surface is considered. In this work, we analyse some significant HAS data for polyatomic conducting surfaces and overlayers, demonstrating the specific role of high-energy phonons in the measured mass-enhancement factor λ.

This work is organized as follows. In Section 2, a brief account of the DW factor evaluated in terms of the electron–phonon interaction is provided. In Section 3, several examples of the DW exponent displaying a non-linear behavior with the surface temperature from He atom scattering data are analyzed and discussed. First, some conductor surfaces with more than one atom per unit cell and a clear separation between high-energy optical phonons and low-energy phonons (whether acoustic or optical) such as Sb(111) and Bi(111). Second, a similar analysis is carried out for a polyatomic conducting surface like that of Sb₂Te₃ (111). And third, this analysis is extended to the case of soft metal overlayers on a stiffer substrate. An interesting question is whether the electron–phonon interaction of the metal overlayer, basically related to its electron band-structure at the Fermi level, receives a contribution from the stiffer, high-energy phonons borrowed from the substrate. The temperature dependence of the HAS DW exponent measured for Cs(110) ultrathin films on a Cu(111) overlayer for a growing number n of Cs atomic layers, and similarly for Pb(111) ultrathin films also on a Cu(111) substrate shows that this is the case. Finally, in Section 4 some conclusions are presented and new directions along this line are pointed out.

2 Debye–Waller factor evaluated in terms of the electron–phonon interaction

In the case of atom-surface scattering in the quantum mechanical limit, and in particular for He atom scattering, the thermal attenuation of all quantum features is governed by a Debye–Waller (D–W) factor of the form $\exp\{-2W(k_f,k_i,T)\}$ where k_i and k_f are the incident and final wave vectors of the He atom projectile. This implies that, for example, the intensity of a diffraction peak is expressed as the multiplicative factor[13,14]

$$I(T) = I_0 \exp\{-2W(k_f,k_i,T)\}, \tag{1}$$

where I_0 is the intensity the peak would have at $T = 0$ in the absence of zero-point motion, *i.e.*, in the rigid lattice limit. In general due to the effects of quantum mechanical zero point motion $I_0 > I\,(T = 0)$.

The exponent of the Debye–Waller factor is expressed as

$$2W(\mathbf{k}_f,\mathbf{k}_i,T) = \langle(\Delta k \cdot \mathbf{u})^2\rangle_T, \tag{2}$$

where $\Delta\mathbf{k} = \mathbf{k}_f - \mathbf{k}_i$ is the scattering vector, $\mathbf{u}$ is the effective vibrational displacement experienced by the projectile atom upon collision, and $\langle\cdots\rangle_T$ denotes the thermal average.

It has long been recognized that when atoms scatter from surfaces, and in particular for He atom scattering, the atoms do not scatter from the atomic cores but rather scatter from the electron cloud that extends outward above the terminal layer of the target crystal.[13] The collision of the projectile atom with the electron cloud then senses the surface cores and their vibrations through the e–ph interaction. The relation of He atom scattering to the e–ph coupling constant was first rigorously demonstrated in the inelastic spectra of He reflected from multiple layers of Pb adsorbed on a Cu(111) substrate.[1,15] There it was shown that the intensity of the inelastic scattering features due to excitation of a surface phonon mode having frequency $\omega_{Q,\nu}$ is directly proportional to the mode components $\lambda_{Q,\nu}$ of the e–ph coupling constant λ. In the above the frequency of a surface phonon mode $\omega_{Q,\nu}$ depends on its parallel wave vector $\mathbf{Q}$ and branch index ν. The e–ph coupling constant λ of Eliashberg is related to the average over the mode components according to $\lambda = \sum_{\mathbf{Q},\nu} \lambda_{\mathbf{Q},\nu}/3N$ where N is the total number of atoms in the target and $3N$ is the total number of phonon modes.[16]

More recently, this inelastic theory has been more fully developed to include elastic as well as inelastic scattering where it is shown that a general expression for the DW exponent in terms of the e–ph interaction appears as[2]

$$2W(\mathbf{k}_f, \mathbf{k}_i, T) = 2\mathcal{N}(E_F)\frac{\hbar^2 k_{iz}^2}{m_e^* \phi}\hbar\omega_0\left\{n_{BE}(\omega_0, T) + \frac{1}{2}\right\}\lambda_{HAS}, \tag{3}$$

where $\mathcal{N}(E_F)$ is the electronic density of electron states at the Fermi surface, m_e^* is the electron effective mass and ϕ is the work function, k_{iz} is the component normal to the surface of the incident atom wavevector in a specular scattering geometry, ω_0 is an average phonon frequency, and $n_{BE}(\omega_0,T)$ is the Bose–Einstein function for a phonon of frequency ω_0 at temperature T. With λ_{HAS} it is meant λ as derived from HAS DW measurements.

The simplest assumption is to expand the Bose–Einstein function to first order where it takes the value $\hbar\omega_{Q,\nu}/k_B T$, an assumption that depends on all phonon energies being less

23136 | *Phys. Chem. Chem. Phys.*, 2022, **24**, 23135–23141

This journal is © the Owner Societies 2022

PCCP

Paper

than the temperature, $\hbar\omega_{Q,\nu} < k_BT$. The DW exponent then becomes

$$2W(\mathbf{k}_f, \mathbf{k}_i, T) = 2\mathcal{N}(E_F)\frac{\hbar^2 k_{iz}^2}{m_e^*\phi}k_B T\lambda_{\text{HAS}}. \qquad (4)$$

Since only low energy phonon modes are included, eqn (4) is linear in T and expressed in terms of the e–ph coupling constant λ_{HAS}. Eqn (4) has been successfully used to obtain values of λ_{HAS} for a large number of conducting surfaces including simple metals, metallic overlayers, chalcogenides and topological surfaces.[3–5]

If it is assumed that the entire phonon spectrum is dominated by a single dispersionless optical frequency ω_0 then eqn (3) is written again for clarity

$$2W(\mathbf{k}_f, \mathbf{k}_i, T) = 2\mathcal{N}(E_F)\frac{\hbar^2 k_{iz}^2}{m_e^*\phi}\hbar\omega_0\left\{n_{\text{BE}}(\omega_0, T) + \frac{1}{2}\right\}\lambda_{\text{HAS}}, \quad (5)$$

Eqn (5) has been used to extract values of λ_{HAS} for a variety of systems in which single-layer graphene is supported on metal substrates.[11] The case of graphene is a bit unusual in that it has the usual low energy acoustic modes, but also has very high energy optical modes. Calandra and Mauri have shown that the optical modes of graphene make an important contribution to the e–ph constant λ and they suggested as a good approximation the assumption that the important optical modes can be represented by a single frequency $\hbar\omega_0 = 160$ meV.[17]

For a surface 2D free-electron gas we can write $2\mathcal{N}(E_F)\hbar^2/m_e^* = a_c n_{\text{sat}}/\pi$, with n_{sat} being the number of surface layers contributing to the surface electron–phonon interaction and a_c

the area of the surface unit cell. The HAS DW exponent becomes

$$2W(\mathbf{k}_f, \mathbf{k}_i, T) = \frac{a_c k_{iz}^2}{\pi\phi}n_{\text{sat}}\lambda_{\text{HAS}}\left\{A\hbar\omega_1 \coth\left(\frac{\hbar\omega_1}{2k_B T}\right)\right.$$
$$\left. + (1-A)\hbar\omega_2 \coth\left(\frac{\hbar\omega_1}{2k_B T}\right)\right\}, \quad \omega_2 > \omega_1$$
$$(6)$$

where the electron–phonon mass-enhancement factor λ_{HAS} results from the sum of the low-energy and high-energy phonon contributions, $\lambda_1 = A\lambda_{\text{HAS}}$ and $\lambda_2 = (1-A)\lambda_{\text{HAS}}$, so that $\lambda_1 + \lambda_2 = \lambda_{\text{HAS}}$. The weight A of the low-energy phonons shall work as a fitting parameter in the following analysis.

Note that for $\omega_2 \gg \omega_1$ such that there is a temperature domain where $\hbar\omega_2/2k_B \gg T \gg \hbar\omega_1/2k_B$, the first term in graph parenthesis can be approximated by $2k_B T\lambda_1$, while the second term is approximately constant

$$2W(\mathbf{k}_f, \mathbf{k}_i, T) \equiv \frac{a_c k_{iz}^2}{\pi\phi}n_{\text{sat}}\lambda_{\text{HAS}}[2\lambda_1 k_B T + \hbar\omega_2\lambda_2],$$
$$\hbar\omega_2 \gg k_B T \gg \hbar\omega_1, \qquad (7)$$

which shows that in this intermediate temperature domain $2W$ is linear in T with a slope proportional to the e–ph coupling of the low-energy modes λ_1. In the high-temperature limit, $T \gg \hbar\omega_2/2k_B$,

$$2W(\mathbf{k}_f, \mathbf{k}_i, T) \simeq \frac{a_c k_{iz}^2}{\pi\phi}n_{\text{sat}}(2\lambda_{\text{HAS}}k_B T), \quad k_B T > \hbar\omega_2, \qquad (8)$$

that is, the DW exponent becomes linear in T with a slope proportional to the total λ_{HAS}. In general, an accurate fit of the experimental $2W(T)$ allows to evaluate separately the contributions of the low- and high-energy phonons to the total
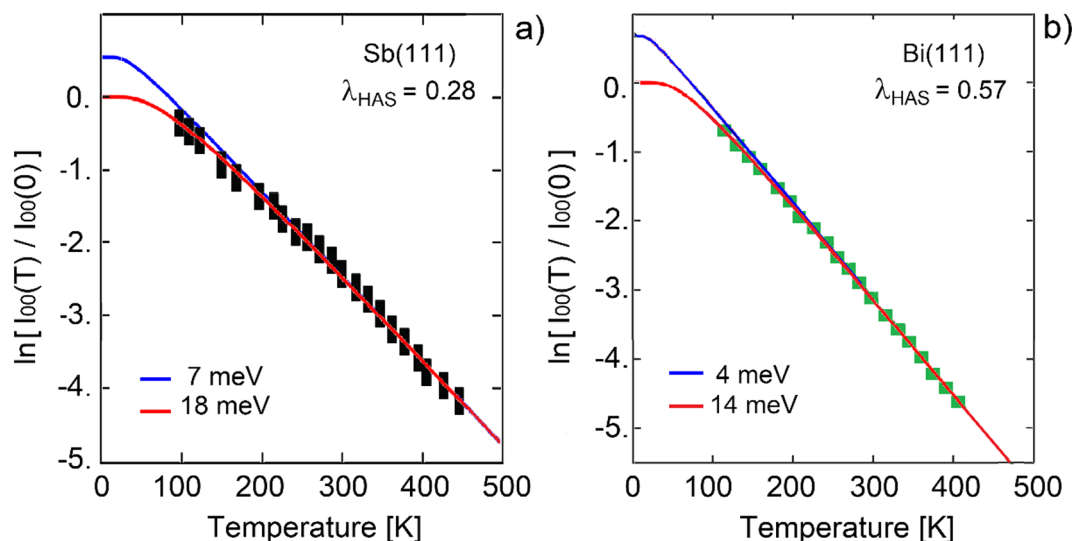

Fig. 1 The DW exponent as a function of surface temperature for the specular diffraction peak of He atom scattering from Sb(111) and Bi(111).[18] The incident energy is $E_i = 24$ meV and the specular angle is 45.75°. For Sb(111) we have $\lambda^{\text{acoustic}} + \lambda^{\text{optical}} = \lambda_{\text{HAS}} = 0.28$ and for Bi(111), $\lambda_{\text{HAS}} = 0.57$. The best fits including only optical phonons (red lines), of average energy of 18 meV for Sb(111) and 14 meV for Bi(111), reproduce better the HAS data than those including only acoustic phonons (blue curves) of maximum energy of 7 and 4 meV, respectively. This qualitatively shows the dominant role of optical phonons in the electron–phonon interaction.

This journal is © the Owner Societies 2022

Phys. Chem. Chem. Phys., 2022, **24**, 23135–23141 | **23137**

electron–phonon mass-enhancement factor λ_{HAS}. In the following examples, it appears that in general high-energy phonons are prominent in the total e–ph interaction, as expected and observed from the intensities of inelastic HAS peaks for the optical modes of Bi(111).[15]

3 Examples of DW exponents that are non-linear in Temperature from He atom scattering

3.1 Optical *versus* acoustic phonons

In the case of conductor surfaces with more than one atom per unit cell and a clear separation between high-energy optical phonons and low-energy phonons (whether acoustic or optical), an increase of slope of $2W(\mathbf{k}_f,\mathbf{k}_i,T)$ or $2W(T)$ in order to simplify the notation is observed in the intermediate temperature region according to eqn (7). This is illustrated for Sb(111) and Bi(111) in Fig. 1.[18] For these crystals, with two atoms per unit cell, there is a gap between the surface optical phonons and the surface acoustic phonons.[19,20] The experimental specular HAS data actually show a slight deviation from linearity in the intermediate temperature region, which can however be appreciated by comparing the best fits with only the optical phonons (red lines), centered around 18 meV for Sb(111)[19] and 14 meV for Bi(111)[20] to those with only acoustic phonons, centered around 7 meV for Sb(111)[19] and 4 meV for Bi(111).[20] The fits with $n_{sat} = 4.7$ for Sb(111), $n_{sat} = 4.5$ for Bi(111), and only optical modes reproduce the experiments at all measured temperatures, whereas the fits with the acoustic modes start deviating below about 200 K (equivalent to $\sim$17 meV) for Sb(111) and 150 K ($\sim$ 13 meV). In these materials it can be concluded that the values of λ_{HAS} (0.28 and 0.57, respectively[3]), previously derived from $2W(T)$ in the linear approximation, are mostly due to the surface optical modes. This is consistent with the observation of comparatively intense inelastic HAS peaks in the optical region of both surfaces.[20,21] A more quantitative conclusion about the actual weights of acoustic and optical modes in the total mass-enhancement factor would require much smaller error bars in the HAS $2W(T)$ data, than those reproduced in Fig. 1, *e.g.*, as it would be possibly obtained with ^{3}He spin-echo spectroscopy.

3.2 He atom scattering from Sb_2Te_3 (111): which optical phonons?

The DW plot has been measured for Sb_2Te_3 (111) as shown in Fig. 2 and this provides an interesting view to illustrate the way that high energy phonon modes enter into the contributions to the e–ph coupling constant for a polyatomic conducting surface.[10,22] The measurements were made at an incident He atom energy E_i = 17.42 meV and at a specular angle of θ_i = 45.75°.

In this case, the surface phonon spectrum as obtained from *ab initio* DFPT calculations[23] and observed by inelastic HAS[22] can be reasonably well split in three regions where the surface phonons are mostly detected by HAS: a high-energy optical
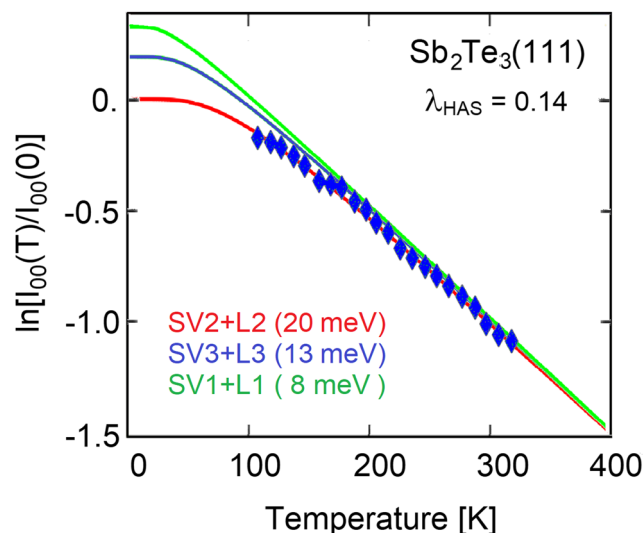

Fig. 2 The DW exponent as a function of surface temperature for the specular diffraction peak of He atom scattering from Sb_2Te_3 (111). Data from ref. 22. The best fit including only the highest optical phonon branches SV2 and L2 involving the Sb layers (see ref. 23) (average energy 20 meV, red line) represents better the HAS data than the fits with only the lower optical branches SV3 and L3 mostly involving the central Te layer (average energy 13 meV, blue line), or only the acoustic branches SV1 and L1 at a maximum energy of 8 meV (green line), although the latter modes move mostly the top Te atoms at the surface layer.

phonon region ($\sim$ 20 meV), with large phonon displacements in the second (Sb) layer in both shear-vertical (SV2) and longitudinal (L2) directions; an intermediate optical phonon region ($\sim$ 13 meV) with displacements more localized on the third atomic (Te) layer (SV3 + L3), and a low-energy, prevalent acoustic phonon region, centered at $\sim$ 8 meV, with larger displacements on the surface atomic layer (SV1 + L1). Also in this case the best fits with $n_{sat} = 12$, corresponding to a Thomas-Fermi screening length extending to about 6 quintuple layer[22] and only high-energy, intermediate-energy, or low-energy phonons shows that the total mass-enhancement factor derived from a pure linear fit, $\lambda_{HAS} = 0.14$[10] is mostly due to the electron–phonon interaction involving the motion of Sb ions within the surface quintuple layer (SV2 and L2 phonon branches[23]). Again, the departure of the fits based on only intermediate- and low-energy phonons from experiment and from the good fit with only high-energy optical phonons starts at about 180 K, which corresponds to $\sim$ 16 meV and just separates the SV2 + L2 from the SV3 + L3 spectral regions.[23]

3.3 Overlayers: the role of substrate

It is now interesting to extend this analysis to the case of soft metal overlayers on a stiffer substrate. An interesting question is whether the e–ph interaction of the metal overlayer, basically related to its electron band-structure at the Fermi level, receives a contribution from the stiffer, high-energy phonons borrowed from the substrate. The temperature dependence of the HAS Debye–Waller exponent measured for Cs(110) ultrathin films on a Cu(111) overlayer for a growing number n of Cs atomic

23138 | *Phys. Chem. Chem. Phys.*, 2022, **24**, 23135–23141

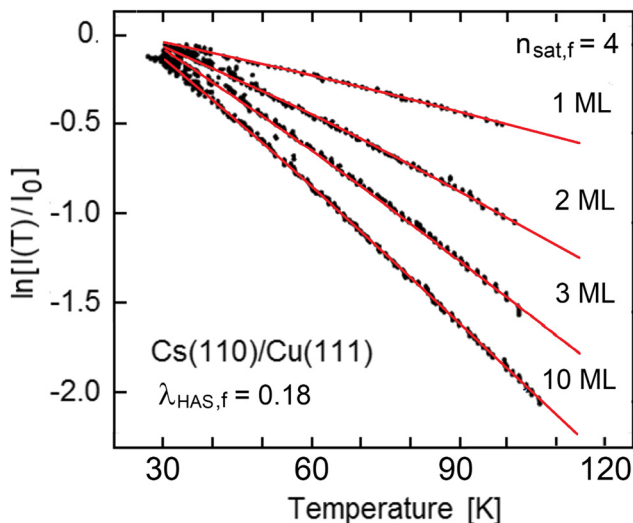This journal is © the Owner Societies 2022

Fig. 3 The DW exponent as a function of surface temperature for the specular diffraction peak of He atom scattering from multiple layers of Cs on Cu(111). The specular angle is $\theta_i = 50.5°$ and the incident energy is $E_i = 28.5$ meV. Data (black dots) are from for Cs overlayers of thickness $n = 1, 2, 3, 10$ ML on Cu(111) ref. 4 and 24. With $\lambda_{HAS,f} = 0.18$ and $\lambda_{HAS,s} = 0.19$ given for Cs and Cu in ref. 2 (Tables 3 and 2), respectively, and $n_{sat,f} = 4$ for Cs films on Cu(111),[2] the best fits (red curves) with eqn (6) and the substitutions of eqn (10) and (11) are obtained with the $A_n = 0.84$ ($n = 1$) and 1 ($n > 1$), and a substrate $n_{sat,s} = 5$.
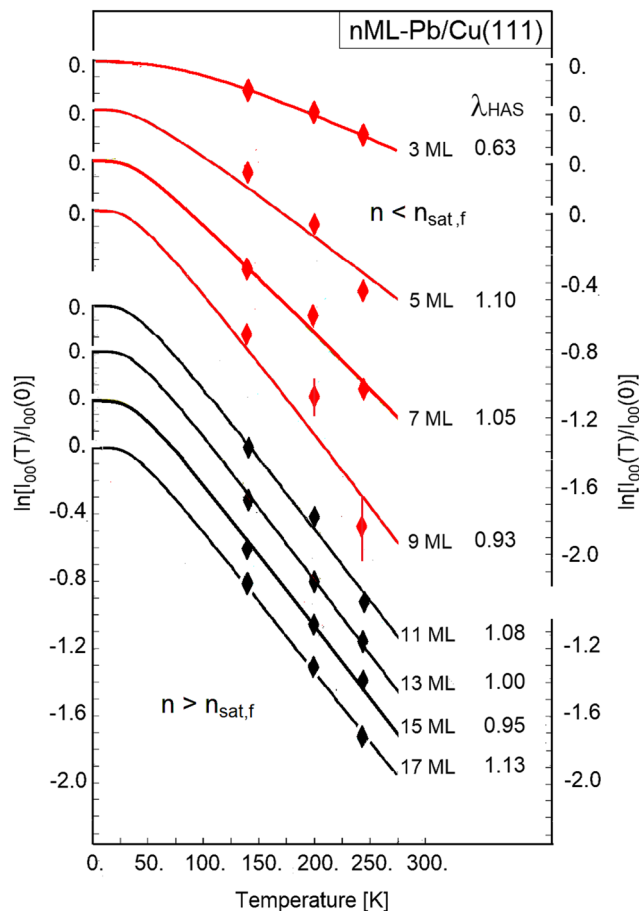

Fig. 4 The DW exponent as a function of surface temperature for the specular diffraction peak of He atom scattering from multiple layers of Pb on Cu(111) for odd values of n from 3 to 17. The specular angle is $\theta_i = 45°$ and the incident energy is $E_i = 5.97$ meV. With an $n_{sat,f}$ of about 9, are also reasonably well fitted, within the fairly large experimental error, by eqn (6), (10) and (11) for both $n < n_{sat,f}$ (red data-points and lines) and $n > n_{sat,f}$ (black data-points and lines), and for the same $n_{sat,s} = 5$ used for the Cs films on Cu(111).

layers in Fig. 3,[2,24] and similarly for Pb(111) ultrathin films also on a Cu(111) substrate[2,25] in Fig. 4, actually provides evidence for this effect.

Both examples show that the slope of $2W(T)$ versus temperature increases with the number n of the atomic layers as long as it does not exceed the saturation number of the film, $n_{sat,f}$.[3] This is due to the increase with n of the number of electronic states at the Fermi level of the film (see, e.g., ref. 25) as well as of the number of its phonon modes. On the other hand, by considering that the saturation number represents the range from (and normal to) the surface of the e–ph interaction, when $n < n_{sat,f}$ the substrate layers near the interface will also contribute to the surface electron–phonon coupling, and for $n = 0$ the saturation number should just become that of the substrate surface, $n_{sat,s}$. Thus, in order to discuss a possible role of the substrate in the actual value of λ_{HAS}, we introduce an n-dependent saturation number $n_{sat}(n)$ interpolating $n_{sat,f}$ for $n \geq n_{sat,f}$ to $n_{sat,s}$ for $n = 0$,

$$n_{sat}(n) = n_{sat,s} + (n_{sat,f} - n_{sat,s})\min(n/n_{sat,f}, 1). \quad (9)$$

Clearly, $n_{sat}(n_{sat,f}) = n_{sat,f}$ and $n_{sat}(0) = n_{sat,s}$. On this basis, we adapt eqn (6) to the case of supported ultra-thin films with the substitutions

$$\lambda_{HAS}n_sA \rightarrow \lambda_{HAS,f}\min(n,n_{sat}(n))A_n/d_n \equiv \lambda_f(n),$$
$$\lambda_{HAS}n_s(1 - A) \rightarrow \lambda_{HAS,s}(n_{sat}(n) - n)(1 - A_n)/d_n \equiv \lambda_s(n), \quad (10)$$

with

$$d_n = \min(n,n_{sat}(n))A_n + (n_{sat}(n) - n)(1 - A_n), \quad (11)$$

with A_n playing the role of a fitting parameter for each thickness, n. In eqn (10), $\lambda_{HAS,f}$ and $\lambda_{HAS,s}$ are the mass-enhancement factors of the film at saturation and of the substrate as derived from HAS DW data in the 2D approximation,[3] respectively, and $\lambda_f(n)$ and $\lambda_s(n)$ are the thickness-dependent components (with indices f and s referring to film and substrate, respectively) of the mass-enhancement factor $\lambda_{HAS}(n)$ of the n-layer-film/substrate system

$$\lambda_{HAS}(n) = \lambda_f(n) + \lambda_s(n). \quad (12)$$

It is easily seen that this is what is directly obtained from the HAS-DW data for each thickness n, and that $\lambda_{HAS}(n_{sat,f}) = \lambda_{HAS,f}$, and $\lambda_{HAS}(0) \equiv \lambda_{HAS,s}$.

Fig. 3 displays the experimental data for the HAS DW exponent $2W(T)$ (black dots) for Cs overlayers of thickness $n = 1, 2, 3, 10$ ML on Cu(111).[4] The single Cs monolayer on Cu(111) behaves as a wetting layer, with a SV phonon frequency of $\omega_{f1} = 6.5$ meV,[26] which is larger than the maximum frequency

of Cs ($\omega_f = 4.3$ meV[25]) here adopted for the films with $n > 1$. For the substrate we use the highest surface mode (S2) average frequency of 28 meV.[27] With $\lambda_{HAS,f} = 0.18$ and $\lambda_{HAS,s} = 0.19$ given for Cs and Cu in ref. 2 (Tables 3 and 2), respectively, and $n_{sat,f} = 4$ for Cs films on Cu(111),[2] the best fits (red curves) with eqn (6) and the substitutions of eqn (10) and (11) are obtained with the $A_n = 0.84$ ($n = 1$) and 1 ($n > 1$), and a substrate $n_{sat,s} = 5$. The latter value is considerably smaller than the value for the free Cu(111) surface, $n_s = 8.5$, in ref. 2 (Table 2), which can be attributed to the charge transfer from the film due to the work function difference. The sequence of the best-fit values of A_n for $n > 1$ indicates a full independence (decoupling) of the Cs film e–ph interaction of (from) the high-energy substrate vibrations. This is reflected in the sequence of $\lambda_{HAS}(1)$, which are all equal to the saturation value 0.18, except for $\lambda_{HAS}(n)$ which is slightly larger. This agrees with the approximate linearity with $n < n_{sat}$ of the parameter α^2, observed in Fig. 3(b) and 5(b) for thin alkali films on different transition-metal substrates.

This is not so for Pb films grown on Cu(111). The experimental HAS data for the DW exponent plotted in Fig. 4 as a function of temperature for odd values of n from 3 to 17 (the Pb films, after forming a wetting monolayer, tend to grow as a bilayer sequence[2]) with an $n_{sat,f}$ of about 9, are also reasonably well fitted, within the fairly large experimental error, by eqn (6), (10) and (11). This holds for both $n < n_{sat,f}$ (red data-points and lines) and $n > n_{sat,f}$ (black data-points and lines), and for the same $n_{sat,s} = 5$ used for the Cs films on Cu(111). In this case the highest average optical surface phonon frequency of Pb layers (~ 9 meV[28]) is used for ω_f, while for $\lambda_{HAS,f}$, whose experimental HAS value displays some oscillations above n_{sat} an average saturation value of 1.1 is used. It appears that at $n = 3$ ($A_n = 0.5$), the contribution of the substrate phonon to the e–ph coupling of the Pb film is 50%, and therefore equal to that of the film optical phonons, and survives (10%, i.e., $A_n = 0.9$) for $n > 3$ up to saturation. The dynamical decoupling occurs above saturation. The observed oscillations of the experimental $\lambda_{HAS}(n)$ for $n > n_{sat}$ are likely to be due to the quantum-size effect,[29] rather than to a residual effect of substrate dynamics. The corresponding sequence of $\lambda_{HAS}(n)$ turns out to be in remarkably good agreement with the experimental values, apart from the oscillations mentioned above. All the information required is collected in Table 1.

4 Conclusions

In this work we have analysed the deviations from linearity of the DW exponent as a function of temperature as observed in He atom scattering from conducting surfaces and shown them to be an effect of the prominence of optical surface phonons. For sufficiently large temperatures, meaning T comparable or greater than the Debye temperature, the DW exponent $2W^{eff}(\mathbf{k}_f,\mathbf{k}_i,T)$ is essentially linear in T as in eqn (8). However, eqn (2) shows that all phonon modes which have polarization components parallel to Δk contribute, even high energy modes which are neglected in the standard treatments. Here it is demonstrated that the electron–phonon interaction method of treating the DW factor allows one to readily estimate the contributions of high energy phonon modes such as, for example, optical modes.

One effect of including such high energy modes is that it can lead to non-linear behavior in $2W^{eff}(\mathbf{k}_f,\mathbf{k}_i,T)$, e.g., different from the standard linear behavior exhibited in eqn (8). These conclusions are supported by calculations for five different surface target systems. These consist of two ordered metallic systems with non-Bravais lattices that contain optical modes in their phonon dispersion relations, one rather exotic layered system containing a single layer of graphene, and two systems involving multiple layered growth of the "soft" metals Cs and Pb deposited on a Cu(111) substrate. In all of these cases small non-linearities of $2W^{eff}(\mathbf{k}_f,\mathbf{k}_i,T)$ can be explained by contributions due to high energy phonon modes. This work indicates that non-linear behavior as a function of T in the DW exponent at high temperature may, in some cases, be explained by the effects of high energy modes, e.g., optical modes, which are usually neglected.

Demonstrating a specific role of the substrate in determining the electron–phonon interaction of an ultrathin films clearly opens new possibilities in the design of superconducting nanostructures and nanodevices.

Conflicts of interest

There are no conflicts to declare.

Acknowledgements

Notes and references

1 I. Y. Sklyadneva, G. Benedek, E. V. Chulkov, P. M. Echenique, R. Heid, K.-P. Bohnen and J. P. Toennies, Mode-selected electron–phonon coupling in superconducting Pb nanofilms determined from He atom scattering, *Phys. Rev. Lett.*, 2011, **107**, 095502.

2 J. R. Manson, G. Benedek and S. Miret-Artés, Atom scattering as a probe of the surface electron–phonon interaction at conducting surfaces, *Surf. Sci. Rep.*, 2022, **77**, 100552.

Table 1 Role of the substrate in the mass-enhancement factor of supported films. For the system n-Cs/Cu(111) ($n = 1, 2, 3, 10$) we have used: $\omega_f(\omega_{fl}) = 4.2^{25}$ (6.5^{26}); $\omega_s = 28$ meV;[27] $n_{sat,f} = 4$,[2] $n_{sat,s} = 5$; $\lambda_{HAS,f} = 0.18$,[2] $\lambda_{HAS,s} = 0.19$. For the system n-Pb/Cu(111) ($n = 3, 5, 7, 9, 11$) we have used: $\omega_f = 9$ meV,[28] $\omega_s = 28$ meV;[27] $n_{sat,f} = 9$,[2] $n_{sat,s} = 5$; $\lambda_{HAS,f} = 1.1$,[2] $\lambda_{HAS,s} = 0.19$.[2]

	n-Cs/Cu(111)				n-Pb/Cu(111)				
n	1	2	3	10	3	5	7	9	11
A_n	0.84	1.	1.	1.	0.5	0.9	0.9	0.9	1.
$\lambda_f(n)$	0.11	0.18	0.18	0.18	0.52	1.05	1.08	1.1	1.1
$\lambda_s(n)$	0.074	0.	0.	0.	0.10	0.01	0.	0.	0.
$\lambda_{HAS}(n)$	0.184	0.18	0.18	0.18	0.62	1.06	1.08	1.1	1.1
λ_{HAS}^{exp}	0.18	0.18	0.18	0.18	0.63	1.10	1.05	0.93	1.08

23140 | *Phys. Chem. Chem. Phys.*, 2022, **24**, 23135–23141

This journal is © the Owner Societies 2022

3 J. R. Manson, G. Benedek and S. Miret-Artés, Electron–phonon coupling strength at metal surfaces directly determined from the helium atom scattering Debye–Waller Factor, *J. Phys. Chem. Lett.*, 2016, **7**, 1016; Erratum: 2016, 7, 1691.

4 G. Benedek, S. Miret-Artés, J. P. Toennies and J. R. Manson, Electron–phonon coupling constant of metallic overlayers from specular He-atom scattering, *J. Phys. Chem. Lett.*, 2018, **9**, 76.

5 G. Benedek, S. Miret-Artés, J. R. Manson, A. Ruckhofer, W. E. Ernst and A. Tamtögl, Origin of the electron–phonon interaction of topological semimetal surfaces measured with helium atom scattering, *J. Phys. Chem. Lett.*, 2020, **11**, 1927.

6 A. Ruckhofer, D. Campi, M. Bremholm, P. Hofmann, G. Benedek, M. Bernasconi, W. E. Ernst and A. Tamtögl, THz surface excitations and electron–phonon coupling in $Bi_2Se_3(111)$ from helium atom scattering, *Phys. Rev. Res.*, 2020, **2**, 023186.

7 G. Anemone, M. Garnica, M. Zappia, P. Casado Aguilar, A. Al Taleb, C.-N. Kuo, C. S. Lue, A. Politano, G. Benedek, A. L. Vázquez de Parga, R. Miranda and D. Farías, Experimental determination of surface thermal expansion and electron–phonon coupling constant of 1T-PtTe2, *2D Mater.*, 2020, **7**, 025007.

8 G. Benedek, J. R. Manson and S. Miret-Artés, The electron–phonon interaction of low-dimensional and multi-dimensional materials from he atom scattering, *Adv. Mater.*, 2020, **32**, 2002072.

9 G. Anemone, P. Casado Aguilar, M. Garnica, F. Calleja, A. Al Taleb, C.-N. Kuo, C. S. Lue, A. Politano, A. L. Vázquez de Parga, G. Benedek, D. Farías and R. Miranda, Electron–phonon coupling in superconducting 1T-PdTe2, *npj 2D Mater. Appl.*, 2021, **5**, 25.

10 G. Benedek, J. R. Manson, S. Miret-Artés, A. Ruckhofer, W. E. Ernst, A. Tamtögl and J. P. Toennies, Measuring the electron–phonon interaction in two-dimensional superconductors with He atom scattering, *Condens. Matter*, 2020, **5**, 79 (2020). Erratum: Condens. Matter, 2021, 6, 54.

11 G. Benedek, J. R. Manson and S. Miret-Artés, The electron–phonon coupling constant for single-layer graphene on metal substrates determined from he atom scattering, *Phys. Chem. Chem. Phys.*, 2021, **23**, 7553.

12 B. Holst, G. N. Alexandrowicz, N. Avidor, G. Benedek, G. Bracco, W. E. Ernst, D. Farías, A. Jardine, J. R. Manson, R. Marquardt, S. Miret-Artés, A. Tamtögl, J. W. Wells and W. Allison, Material properties particularly suited to be measured with helium scattering: Selected examples from 2D materials, van der Waals heterostructures, glassy materials, catalytic substrates, topological insulators and superconducting radio frequency materials, *Phys. Chem. Chem. Phys.*, 2021, **23**, 7653.

13 G. Benedek and J. P. Toennies, Atomic scale dynamics at surfaces: Theory and experimental studies with helium atom scattering, *Springer Series in Surface Sciences*, Springer Press, Heidelberg, 2018, vol. 63, ISBN 978-3-662-56443-1.

14 *Springer Series in Surface Sciences*, ed. E. Hulpke, Springer Press, Heidelberg, 1992, vol. 27.

15 G. Benedek, M. Bernasconi, K.-P. Bohnen, D. Campi, E. V. Chulkov, P. M. Echenique, R. Heid, I. Yu. Sklyadneva and J. P. Toennies, Unveiling mode-selected electron–phonon interactions in metal films by helium atom scattering, *Phys. Chem. Chem. Phys.*, 2014, **16**, 7159.

16 P. B. Allen, Neutron spectroscopy of superconductors, *Phys. Rev. B: Solid State*, 1972, **6**, 2577.

17 M. Calandra and F. Mauri, Electron–phonon coupling and electron self-energy in electron-doped graphene: Calculation of angular-resolved photoemission spectra, *Phys. Rev. B: Condens. Matter Mater. Phys.*, 2007, **76**, 205411.

18 A. Tamtögl, M. Mayrhofer-Reinhartshuber, P. Kraus and W. E. Ernst, Surface Debye temperature and vibrational dynamics of antimony (111) from helium atom scattering measurements, *Surf. Sci.*, 2013, **617**, 225.

19 D. Campi, M. Bernasconi and G. Benedek, Phonons and electron–phonon interaction at the Sb(111) surface, *Phys. Rev. B: Condens. Matter Mater. Phys.*, 2012, **86**, 075446.

20 A. Tamtögl, P. Kraus, M. Mayrhofer-Reinhartshuber, W. E. Ernst, D. Campi, M. Bernasconi and G. Benedek, Surface and sub-surface phonons of Bi(111) measured with helium atom scattering, *Phys. Rev. B: Condens. Matter Mater. Phys.*, 2013, **87**, 035410; Erratum: Phys. Rev. B, 2013, 87, 159906.

21 A. Tamtögl, P. Kraus, M. Mayrhofer-Reinhartshuber, G. Benedek, M. Bernasconi, D. Dragoni and W. E. Ernst, Surface phonons and CDW excitations by helium atom scattering from Sb(111), *npj Quantum Mater.*, 2019, **4**, 28.

22 A. Ruckhofer, S. Halbritter, H. E. Lund, A. Julie, U. Holt, M. Bianchi, M. Bremholm, G. Benedek, P. Hofmann, W. E. Ernst and A. Tamtögl, Inelastic helium atom scattering from $Sb_2Te_3(111)$: Surface phonon dispersion, kinematical focusing and surfing, *Phys. Chem. Chem. Phys.*, 2021, **23**, 7806.

23 D. Campi, M. Bernasconi and G. Benedek, *Ab initio* calculation of surface phonons at the $Sb_2Te_3(111)$ surface, *Surf. Sci.*, 2018, **678**, 38.

24 E. Hulpke, J. Lower and A. Reichmuth, Strain and confined resonances in ultrathin alkali-metal films, *Phys. Rev. B: Condens. Matter Mater. Phys.*, 1996, **53**, 13901.

25 D. Campi, M. Bernasconi, G. Benedek, A. P. Graham and J. P. Toennies, Surface lattice dynamics and electron–phonon interaction in cesium ultra-thin films, *Phys. Chem. Chem. Phys.*, 2017, **19**, 16358.

26 J. P. Gauyacq and A. K. Kazansky, Laser-induced vibrational excitation and desorption in the Cs/Cu(111) and Na/Cu(111) systems, *Surf. Sci.*, 2007, **601**, 5473.

27 G. Benedek, M. Bernasconi, V. Chis, E. Chulkov, P. M. Echenique, B. Hellsing and J. P. Toennies, Theory of surface phonons at metal surfaces: Recent advances, *J. Phys.: Condens. Matter*, 2010, **22**, 084020.

28 J. Braun, P. Ruggerone, G. Zhang, J. P. Toennies and G. Benedek, Surface phonon dispersion curves of thin Pb films on Cu(111), *Phys. Rev. B: Condens. Matter Mater. Phys.*, 2009, **79**, 205423.

29 B. J. Hinch, C. Koziol, J. P. Toennies and G. Zhang, Evidence for quantum size effects observed by helium atom scattering during the growth of Pb on Cu(111), *Europhys. Lett.*, 1989, **10**, 341.

This journal is © the Owner Societies 2022

Phys. Chem. Chem. Phys., 2022, **24**, 23135–23141 | 23141